

## Ion-Scale Solitary Structures in the Solar Wind Observed by Solar Orbiter and Parker Solar Probe

YUFEI YANG,<sup>1</sup> TIMOTHY S. HORBURY,<sup>1</sup> DOMENICO TROTTA,<sup>1,2</sup> LORENZO MATTEINI,<sup>1</sup> JOSEPH WANG,<sup>1</sup> ANDREY FEDOROV,<sup>3</sup>  
PHILIPPE LOUARN,<sup>3</sup> STUART BALE,<sup>4,5</sup> MARC PULUPA,<sup>6</sup> DAVIN E. LARSON,<sup>6</sup> MICHAEL STEVENS,<sup>7</sup> MILAN MAKSIMOVIC,<sup>8</sup>  
YURI KHOTYAINTEV,<sup>9</sup> AND ANDREA LAROSA<sup>10</sup>

<sup>1</sup>*Imperial College London, UK*

<sup>2</sup>*European Space Agency (ESA), Paris, France*

<sup>3</sup>*Institut de Recherche en Astrophysique et Planétologie, CNRS, Université de Toulouse, CNES, Toulouse, France*

<sup>4</sup>*Physics Department, University of California, Berkeley, CA 94720-7300, USA*

<sup>5</sup>*Space Sciences Laboratory, University of California, Berkeley, CA 94720-7450, USA*

<sup>6</sup>*Space Sciences Laboratory, University of California, Berkeley, USA*

<sup>7</sup>*Harvard-Smithsonian Center for Astrophysics, Cambridge, MA, USA*

<sup>8</sup>*CNRS Délégation Île-de-France Ouest et Nord, Meudon, France*

<sup>9</sup>*Swedish Institute of Space Physics, Uppsala, Sweden*

<sup>10</sup>*Consiglio Nazionale delle Ricerche, Bari, Italy*

### ABSTRACT

We investigate a class of ion-scale magnetic solitary structures in the solar wind, characterized by distinct magnetic field enhancements and bipolar rotations over spatial scales of several proton inertial lengths. Previously tentatively identified as Alfvénic solitons, these structures are revisited using high-resolution data from the Solar Orbiter and Parker Solar Probe missions. Using a machine learning-based method, we identified nearly a thousand such structures, providing new insights into their evolution and physical properties. Statistical analysis shows that these structures are more abundant closer to the Sun, with occurrence rates peaking around 30 – 40  $R_{\odot}$  and declining at greater distances, suggesting that they decay. High-cadence measurements reveal that these structures are predominantly found in low-beta environments, with consistent fluctuations in density, velocity, and magnetic field. Magnetic field enhancements are often accompanied by plasma density drops, which, under near pressure balance, limit field increases. This leads to small fractional field enhancements near the Sun (approximately 0.01 at 20  $R_{\odot}$ ), making detection challenging. Magnetic field variance analysis indicates that these structures are primarily oblique to the local magnetic field. Alfvénic velocity-magnetic field correlations suggest that most of these structures propagate sunward in the plasma frame, distinguishing them from typical solar wind fluctuations. We compare these findings with previous studies, discussing possible generation mechanisms and their implications for the turbulent cascade in the near-Sun Alfvénic solar wind. Further high-resolution observations and simulations are needed to fully understand their origins and impacts.

*Keywords:* Solar wind — Magnetic structures — Turbulence

### 1. INTRODUCTION

The solar wind, a continuous supersonic plasma flow from the Sun, serves as an ideal natural laboratory for studying turbulence in collisionless plasmas (Bruno & Carbone 2013). Despite decades of research, fundamental questions remain about the nature of turbulent fluctuations across the cascade and the mechanisms driving energy dissipation in the solar wind. Numerous studies have highlighted the multi-scale nature of solar wind turbulence (e.g., Bruno & Carbone 2013; Verscharen et al. 2019), where energy cascades from large inertial scales, characterized by power-law behavior similar to fluid turbulence (Kolmogorov 1941) and often dominated by highly Alfvénic, outward-propagating fluctuations, to ion and electron kinetic scales, where spectral steepening and kinetic effects emerge. At these smaller kinetic scales, plasma behavior becomes increasingly influenced by ion and electron dynamics, altering the nature of

the fluctuations (e.g., [Matthaeus & Velli 2011](#); [Alexandrova et al. 2013](#)).

A defining feature of turbulence is the statistical self-similarity of fluctuations across scales. However, in the solar wind, this idealized scale invariance breaks down as turbulence exhibits intermittency – regions of localized, non-uniform energy distribution that grow more pronounced as the cascade progresses. Intermittency deviates from Gaussian statistics and often manifests as coherent structures, which localize energy and potentially play a critical role in energy dissipation ([Frisch 1995](#); [Biskamp 2003](#); [Miao et al. 2011](#)). These structures are not merely fluctuations but distinct phenomena associated with specific physical processes, providing valuable insight into the interplay between turbulence and kinetic effects. Particularly at ion scales, such as the ion inertial length ( $\lambda_i = c/\omega_{pi}$ , where  $\omega_{pi} = q_i \sqrt{n_i/(m_i \epsilon_0)}$ ) and the ion Larmor radius ( $\rho_i = V_\perp m_i / (q_i B_0)$ , with  $V_\perp = \sqrt{k_B T_\perp / m_i}$ ), these structures could contribute to plasma heating and particle acceleration and are critical for understanding localized energy transfer and dissipation processes in the solar wind ([Leamon et al. 1998](#); [Bale et al. 2005](#); [Smith et al. 2006](#); [Alexandrova et al. 2013](#)).

In situ observations have revealed a diverse range of ion-scale structures in the solar wind, including current sheets (e.g., [Cattani 2004](#); [Greco & Perri 2014](#); [Osman et al. 2011, 2012](#); [Perri et al. 2012](#)), Alfvén vortices (e.g., [Roberts et al. 2013](#); [Lion et al. 2016](#); [Perrone et al. 2016](#)), and magnetic holes or dark solitons (e.g., [Ryutova & Hagenaar 2007](#); [Perrone et al. 2016](#)). The formation of these structures is often attributed to kinetic instabilities that facilitate energy transfer across scales (e.g., [Verscharen et al. 2019](#)). For example, quasi-static compressive structures, such as magnetic holes and mirror-mode structures, are associated with the mirror-mode instability, occurring in high- $\beta$  plasma under conditions of  $T_\perp > T_\parallel$  ([Soucek & Escoubet 2008](#); [Winterhalter et al. 1994](#); [Zhang et al. 2009](#); [Yao et al. 2013](#)).

In this study, we focus on a different class of ion-scale structures, manifesting as localized, nonlinear wave packets. First identified in Ulysses data as rare events ([Rees et al. 2006](#)), these structures are characterized by clear magnetic field enhancements and bipolar rotations in one or two field components, with a scale size of approximately  $30 \lambda_p$ . They exhibit distinctive banana-shaped magnetic hodograms identified through Minimum Variance Analysis (MVA) ([Sonnerup 1998](#)). Kinetic simulations by [Baumgärtel et al. \(2007\)](#) showed that kinetic solitary structures, resembling obliquely propagating Alfvén wave pulses with quasi-circular or banana-type polarization, may reproduce most observational features reported by [Rees et al. \(2006\)](#). The former analysis using Ulysses data, however, was limited by the temporal resolution of the available plasma instruments, restricting detailed plasma studies within these structures. With recent advancements, high-resolution data from the Parker Solar Probe (PSP) and Solar Orbiter (SO) missions now enable the identification of new candidates across varying heliocentric distances, as illustrated by the examples in [Figure 1](#). With data from SO and PSP, we can now study the evolution of these structures and reveal unprecedented plasma signatures within them, including proton density, velocity, temperature, and electron density from onboard instruments. We conducted an extensive search through PSP and SO magnetic field data, covering five years (2019–2023), with a particular focus on PSP encounters within 0.25 AU. This effort has led to the identification of nearly a thousand such structures, enabling statistical analysis to address key questions: What are the physical characteristics of these solitary structures? How do they form and evolve within the solar wind? How do they contribute to the broader solar wind turbulence?

## 2. DATA AND METHODS

The data used in this study for the identification and analysis of solitary structures in the solar wind were sourced from SO data included magnetic field measurements from the magnetometer (MAG) ([Horbury et al. 2020](#)), proton velocity, density, and temperature from the Solar Wind Analyzer - Proton Alpha Sensor (SWA-PAS) ([Owen et al. 2020](#)), and high-resolution electron density from the Radio and Plasma Waves (RPW) ([Maksimovic et al. 2020](#); [Khotyaintsev et al. 2021](#)) instrument. PSP data included magnetic field measurements and electron density from the FIELDS suite ([Bale et al. 2016](#)), along with proton velocity, density, and temperature from the Solar Wind Electrons Alphas and Protons - Solar Probe Analyzers (SWEAP-SPAN-Ion) instrument ([Kasper et al. 2016](#)).

Traditional methods for identifying ion-scale structures, such as wavelet transforms followed with non-Gaussianity analysis, (e.g., [Perrone et al. 2016, 2017](#)) and Partial Variance of Increments (e.g., [Greco et al. 2018](#)), are effective but require substantial manual effort when analyzing extensive solar wind datasets from modern missions. This challenge

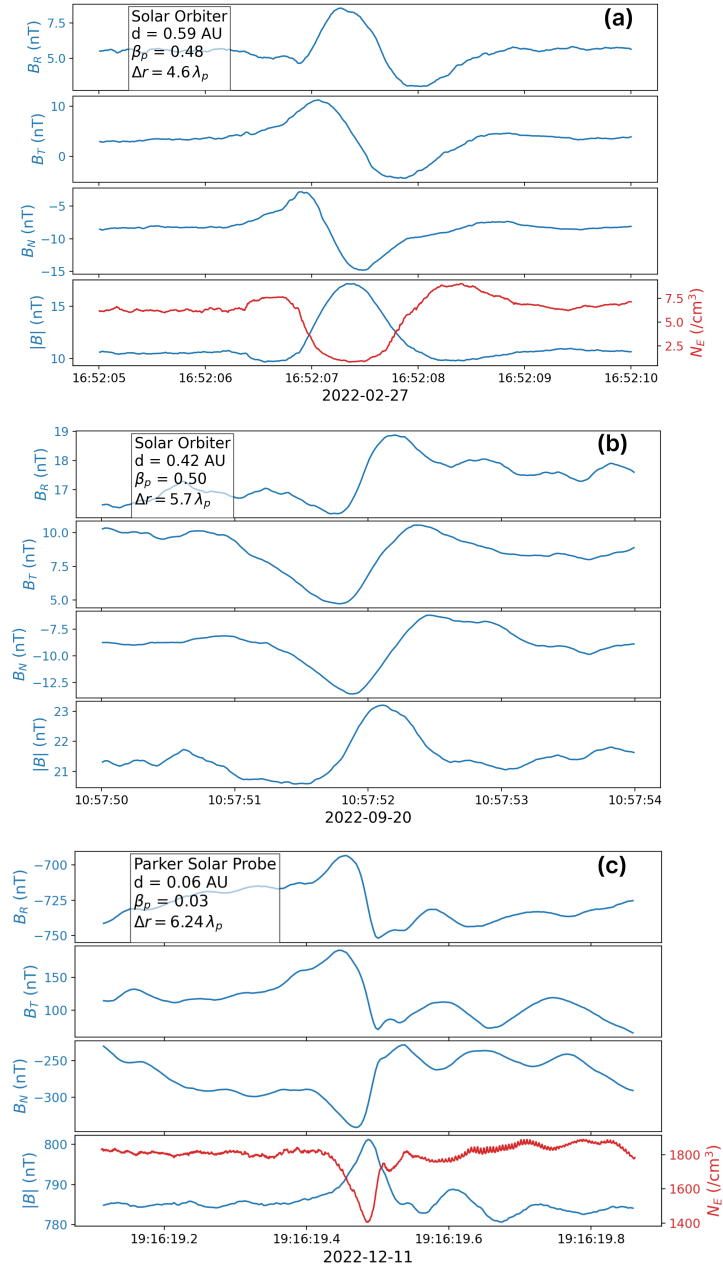


**Figure 1.** Examples of ion-scale solitary structures observed by Solar Orbiter (a, b) and Parker Solar Probe (c), showing magnetic field profiles and plasma density in the RTN frame. Each panel presents  $B_R$ ,  $B_T$ ,  $B_N$ ,  $|B|$ , and high-resolution electron number density  $N_E$  during the event. The text box specifies the heliocentric distance to the Sun in AU, the proton beta ( $\beta_p$ ), and the event width normalized by the proton inertial length ( $\lambda_p$ ) for each event. Note:  $N_E$  is not available for event (b).

is particularly pronounced when reviewing datasets from the inner heliosphere, where turbulence further complicates detection. As a promising alternative to traditional methods, we developed a supervised machine learning (ML) classifier to automate the search across years of high-resolution magnetic field data.

Specifically, we constructed a training dataset using traditional intermittency detection methods. Potential sites for these structures were identified by filtering the fractional magnetic field fluctuations  $\delta|B|/\langle|B|\rangle$  around ion scales using wavelet transforms with a Mexican-Hat wavelet as the mother function, selected due to its shape matching the target structure's field enhancement. Time scales were set to 0.5 s (2 Hz) for PSP and 1.0 s (1 Hz) for SO. A stringent

99.99th percentile threshold was applied to the wavelet results from each day of magnetic field data to isolate the most intermittent time windows. These windows were then manually inspected in the original magnetic field data with the MVA and hodogram creation (Sonnerup 1998). Key selection criteria included (1) significant magnetic field enhancement ( $|B|$ ), (2) a clear bipolar rotation in at least one RTN and MVA component with associated variations in others, and (3) well-defined hodogram patterns resembling banana or quasi-circular shapes. This process identified 466 manually verified events – 157 from SO and 309 from PSP – which formed the basis for the training dataset of the ML classifiers. Data augmentation techniques were then applied to expand this training set. We experimented with several ML algorithms, with the Random Forest model (Breiman 2001) demonstrating the highest precision, interpretability, and effectiveness. To prioritize true positives, we applied the model with a conservatively high classification threshold, accepting some missed detections of false negatives in favor of accuracy.

This ML-based identification method led to the discovery of 974 events, significantly enhancing detection efficiency. Detailed statistical analyses of their profiles and characteristics, occurrence and evolution, propagation, and comparisons with non-event periods are discussed in the following section. Since the primary focus of this paper is on the physics results and implications, the details of the ML implementation will be published separately.

### 3. RESULTS

#### 3.1. Profiles and Characteristics

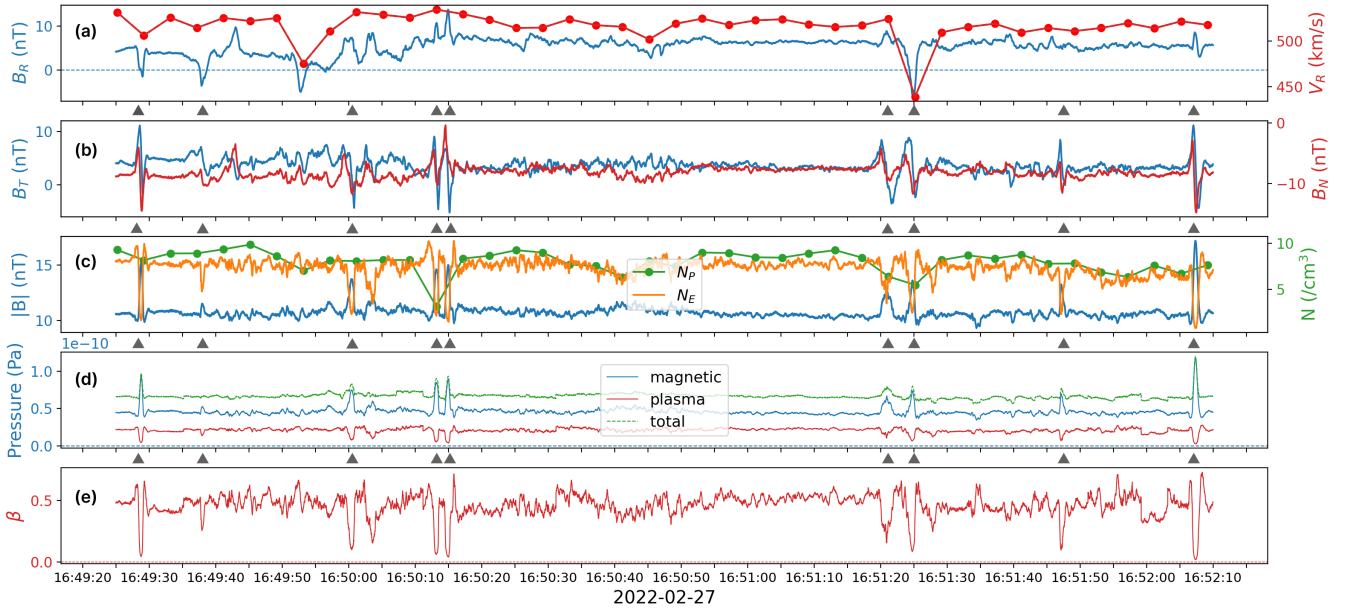


**Figure 2.** An example of a multiple-event period observed by Solar Orbiter. Panels show: (a)  $B_R$  and  $V_R$ , (b)  $B_T$  and  $B_N$ , (c)  $|B|$  and  $N_p$  (proton number density) and  $N_e$  (electron number density), (d) magnetic, plasma (evaluated using high-resolution  $N_e$  and proton temperature) and total pressures, and (e) plasma  $\beta$ , calculated using the magnetic and plasma pressures. Triangles across the panel grid lines indicate the occurrence of each event.

The event illustrated in Figure 1 panel (a) represents a typical, well-defined example observed by SO, lasting approximately 1 second. Its smooth magnetic profile features a pronounced field enhancement resembling a Gaussian ‘blip’ with two dips on either side, closely matching the shape of a Mexican-Hat wavelet function. This enhancement is accompanied by distinct bipolar spikes in all three RTN components, with a return to the initial values, suggesting a solitary structure rather than a boundary crossing. These rotations persist longer than the magnetic field enhancement itself and are clear in the MVA frame, where variance directions are well-defined. A banana-shaped hodogram, observed in the  $B_{\text{int}}$  versus  $B_{\text{max}}$  plot within the MVA frame, aligns with the features reported by Rees et al. (2006), though not explicitly shown here. Additionally, plasma measurements of proton and electron densities reveal that the magnetic field enhancement is often anti-correlated with a plasma density dip, as shown in the fourth panel of

the figure. Correlated electric field fluctuations are also found to accompany these magnetic variations, but these are challenging to interpret given instrumental and spacecraft effects so we do not discuss them in detail in this work. While this example is clear, the final event dataset includes less distinct cases where magnetic profiles are less smooth, and rotations in field components are incomplete or less pronounced relative to background fluctuations. Notably, the turbulent background adds complexity and challenges in consistently applying strict classification criteria for these structures.

Though these events can be isolated, a substantial proportion were found to cluster. Specifically, 94% of events in the PSP dataset and 54% in the SO dataset occurred within 24 hours of another event, and 57% of events in PSP and 38% in SO reoccurred within one hour. This suggests that certain conditions may favor the formation of multiple events. Such multi-event clusters are primarily observed in regions where the background magnetic field is both low and stable, exemplified in Figure 2. The event shown in Figure 1 (a) falls within this period. In panels (b) and (c) of Figure 2, we observe consistent patterns of associated variations among magnetic field profiles and density profiles for this cluster, resembling the single-event example. In panel (d), the prominent magnetic field enhancement, coupled with a modest plasma density drop, results in a more significant increase in magnetic pressure than the decrease in plasma pressure (calculated using higher-resolution electron density as a proxy for proton density and proton temperature data). This suggests that these structures are magnetically dominated, perhaps exhibiting a temporary slight pressure imbalance that leads to an overall pressure increase within the event and a reduction in plasma  $\beta$ , as shown in panel (e) of Figure 2;  $\beta$  remained below 1 throughout this period.

### 3.2. Radial Evolution

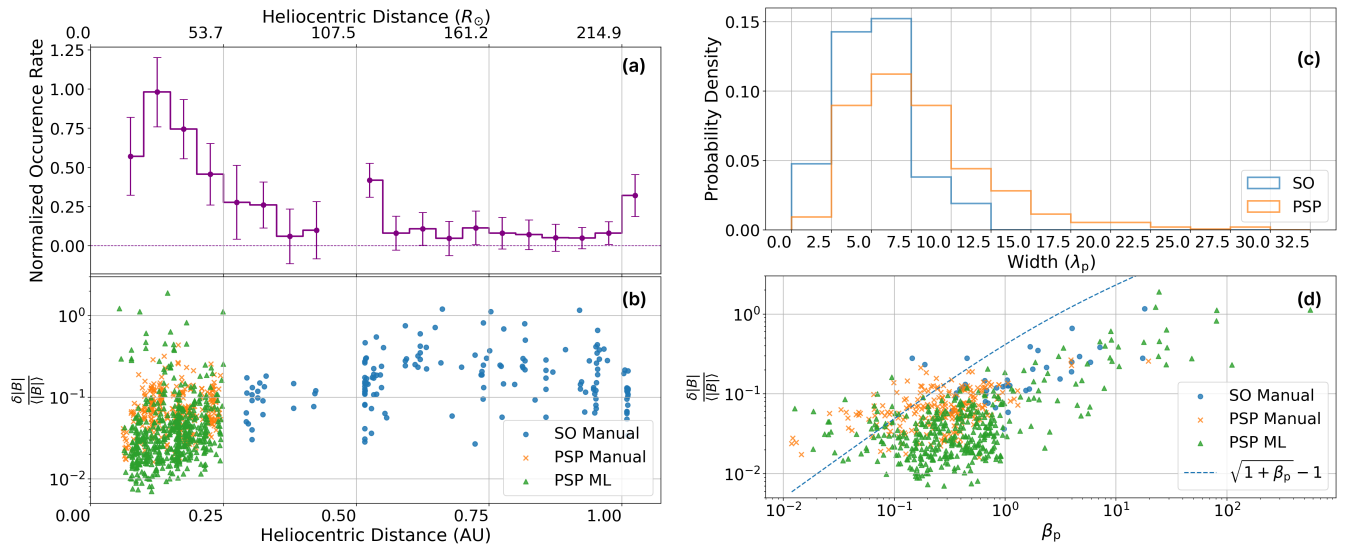


**Figure 3.** Statistical analysis results of the ion-scale solitary structures dataset. (a) Normalized occurrence rate (events/day), representing the aggregated occurrence rate across datasets adjusted for data availability and scaled to address methodological differences, and (b) fractional magnetic field enhancement ( $\delta|B|/|B|$ ), both presented as functions of radial distance. Error bars in (a) represent standard errors, assuming occurrences are Poisson random variables. (c) Normalized distribution of event widths in proton inertial length ( $\lambda_p$ ), with separate frequency plots for events from Solar Orbiter (SO) and Parker Solar Probe (PSP). (d)  $\delta|B|/|B|$  plotted against proton beta ( $\beta_p$ ) for each event. The blue dashed line represents the theoretical upper bound  $\sqrt{1 + \beta_p} - 1$  on  $\delta|B|/|B|$ , restricted by  $\beta_p$  under pressure balance conditions. Legends label data sources by method: manually identified events (SO manual: blue circles; PSP manual: orange crosses) and machine learning-detected events (PSP ML: green triangles).

Figure 1 presents structures observed at varying distances from the Sun: SO examples at 0.6 AU (panel a) and 0.4 AU (panel b), and a closer PSP example at 0.06 AU (panel c). Consistent correlated fluctuations in the magnetic field, density, and electric field are observed across these examples. While not all events are as clear as these, all

exhibit short and smooth magnetic field enhancement with associated bipolar rotations in the components. Notably, the fractional field enhancements ( $\delta|B|/\langle|B|\rangle$ ) typically decrease as heliocentric distance decreases, from  $\sim 0.75$  in example (a),  $\sim 0.09$  in example (b), to  $\sim 0.03$  in example (c). This pattern suggests that the maximum amplitude of magnetic blips is constrained by plasma density drops, assuming total pressure conservation before and during the event. If we assume pressure balance exists inside and outside the structures, then:

$$P_{\text{outside}} = P_B + P_p = P_{\text{inside}} = P'_B + P'_p \quad (1)$$

With plasma density at a minimum of zero, the minimum plasma pressure  $P'_p$  inside the blip is also zero, making the maximum magnetic pressure  $P'_B$  inside the blip:

$$P'_B \leq (1 + \beta)P_B \quad (2)$$

Hence the change in magnetic field strength is limited by:

$$\frac{|B'|}{|B|} \leq \sqrt{\frac{P'_B}{P_B}} = \sqrt{1 + \beta} \quad (3)$$

The fractional change in magnetic field strength can then be expressed as:

$$\frac{\delta|B|}{|B|} \leq \frac{|B'| - |B|}{|B|} = \sqrt{1 + \beta} - 1 \quad (4)$$

The fractional field magnitude enhancement ( $\delta|B|/\langle|B|\rangle$ ) is shown in Figure 3 as a function of proton  $\beta$  where most events satisfy the criteria in Equation 4. This pattern aligns with the observed decrease in  $\delta|B|/\langle|B|\rangle$  with decreasing distance to the Sun for the events, as shown in panel (b) of Figure 3, since lower plasma  $\beta$  values are typically observed in the inner heliosphere. These findings reveal the detection challenges within 0.25 AU, where minimal fractional field enhancements underscore the need for machine learning techniques to identify these structures effectively.

A small fraction of events – 3% for SO and 6% for PSP – exceed the upper limit set by Equation 4. These deviations could arise from slight pressure imbalances in the structures or from limitations in beta estimation and measurement uncertainties. The  $\beta$  values here are calculated solely from proton density, potentially underestimating total plasma pressure by neglecting electron and other ion contributions. Additionally,  $\beta$  values were averaged over longer windows (2–5 seconds) either side of the structures due to the lower cadence of plasma measurements compared to magnetic field data, possibly smoothing out localized variations and contributing to discrepancies.

Although detecting these structures is more challenging closer to the Sun due to lower  $\delta|B|/\langle|B|\rangle$ , our analysis of occurrence rates as a function of heliocentric distance shows they are more abundant nearer to the Sun. These rates represent aggregated event counts per day across datasets, normalized for data availability and scaled to account for methodological differences. The scaling process involved comparing occurrence rates at overlapping distances between machine learning and manual detection methods, as well as between PSP and SO datasets, accounting for variations in wavelet transform scales. Panel (a) of Figure 3 shows the occurrence rate peaks around 0.1 AU. The lower occurrence rates at the smaller distances, within 0.05 AU, suggest that these structures may either form beyond this region or become undetectable in the near-Sun’s turbulent magnetic field environment with its stronger field.

To investigate the physical scales of these events, we approximated the event width by analyzing the temporal width of the magnetic enhancement. A Gaussian fit was applied to the data to extract key parameters, including the amplitude,  $\sigma$ , and the background magnetic field magnitude. The Full Width at Half Maximum derived from the Gaussian fit was used as a measure of the temporal width of the events. As the temporal profiles of the magnetic field components in the RTN frame were observed to remain largely consistent throughout the events, we converted the temporal width into a spatial scale by focusing on the radial width incorporating the relative radial speed between the spacecraft, the solar wind, and the structures, assuming sunward propagation at the local Alfvén speed (see Section 3.3). Spatial widths were further normalized by the proton inertial length ( $\lambda_p$ ) and proton Larmor radius ( $\rho_p$ ) for analysis. While there was no apparent ordering with  $\rho_p$ , there is a clear propensity for widths between 2.5 and 10  $\lambda_p$  as seen Figure 3 (c), broadly consistent with Rees et al. (2006). Widths normalized by  $\rho_p$  were less consistent between

SO and PSP datasets. The relationship between width and amplitude shows a direct correlation when normalized by  $\rho_p$  but displayed less variability and no correlation when normalized by  $\lambda_p$ , supporting the proton inertial length as a more stable scaling metric for defining the width of these structures.

### 3.3. Propagation Analysis

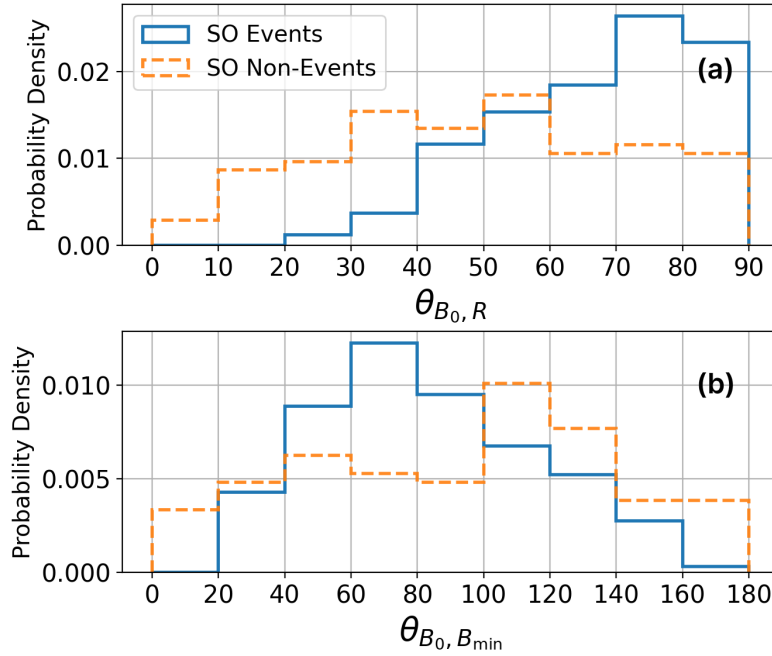


**Figure 4.** Normalized distributions of angles  $\theta$  between (a) the background magnetic field ( $B_0$ ) and the radial direction, and (b)  $B_0$  and the minimum variance direction ( $B_{\min}$ ). Legends, shared across panels, represent events from Solar Orbiter (SO events) and randomly sampled intervals without events (SO non-events).

Magnetic field variance analysis showed large eigenvalue ratios, specifically  $\lambda_{\text{int}}/\lambda_{\text{min}}$  and  $\lambda_{\text{max}}/\lambda_{\text{int}}$ , supporting  $B_{\min}$  as the wavevector. These structures, compared to non-event periods sampled randomly with comparable sizes, are typically detected when the spacecraft’s sampling direction forms larger angles with the background magnetic field ( $B_0$ ). This relationship is most pronounced for SO events at large heliocentric distances. As shown in Figure 4 (a), the structures are predominantly observed during periods with  $\theta(B_0, R)$  near 90 degrees, significantly higher than during non-event periods. The radial direction closely aligns with the sampling direction. The minimum variance directions of the structures  $B_{\min}$  also form large angles with  $B_0$ , as shown in Figure 4 (b), reflecting quasi-perpendicular orientations to  $B_0$  and a distribution distinctly different from non-event periods. PSP events, although less clear, show a similar pattern.

As can be seen from Figure 2 (a), despite the limited plasma time resolution there is clear evidence for velocity variations associated with these events. The positive correlations between  $\delta B_R$  and  $\delta V_R$  within this interval, with a positive background radial field component, is consistent with a sunward propagation direction in an Alfvénic sense, in contrast to most fluctuations in the inner solar system. This sunward propagation sense is generally true for the events, with 568 events from the PSP and 77 from SO exhibiting this trend, while anti-sunward events were comparatively rare, with only 17 detected in PSP and 5 in SO data. Limitations in velocity data, particularly in the SO dataset, restricted analysis for some events (75 out of 157), and the low temporal resolution of velocity data introduced uncertainties in confirming propagation direction for certain structures. This analysis supported the assumption made when evaluating the spatial widths of the blips: additional calculations showed that the propagation direction had minimal impact on the physical width estimation, as the blip speed, approximated as the local Alfvén speed, was

significantly lower compared to both the spacecraft and solar wind speeds.

Additionally, we compared plasma conditions between event and non-event periods. Results indicate that events tended to occur at slightly elevated proton temperatures relative to non-event periods. Both PSP and SO data show consistently higher temperatures for events, suggesting that solitary structures may preferentially form in regions with higher thermal energy. For ambient solar wind speed, PSP data reveals that events occur at a higher average speed (400 km/s vs. 300 km/s) compared to non-events, whereas SO data shows no significant speed separation, with both events and non-events averaging around 400 km/s. This suggests a possible link between faster wind speeds and event occurrence. Plasma beta distribution shows no significant difference between events and non-events, both typically lying within low-beta regions. Temperature anisotropy analysis also reveals no strong association of these structures with proximity to any specific plasma instabilities, such as mirror or fire hose, indicating these structures typically form under stable solar wind conditions without a distinct tendency toward these instabilities.

#### 4. DISCUSSION

The analysis presented here demonstrates that the isolated structures first identified by Rees et al. (2006) beyond 1 AU are significantly more common closer to the Sun but are challenging to detect due to their relatively smaller amplitudes. These structures exhibit well-defined magnetic field profiles with distinct field magnitude enhancements accompanied by sharp decreases in plasma density to very low values. With scales of a few proton inertial lengths, they primarily propagate obliquely to the background magnetic field and display field-velocity correlations opposite to most solar wind in the inner heliosphere, consistent with sunward propagation in an Alfvénic sense.

Variations across the three magnetic field components, indicating both field rotation and compression, distinguish these structures from other purely compressive phenomena, such as magnetic holes or mirror modes, which typically show linear polarization with variations confined to a single direction. The observed behavior aligns with Alfvénic solitons (Mjølhus 1976; Spangler & Sheerin 1982), localized MHD structures driven by transverse magnetic field oscillations and characterized by significant variations in the  $|B|$  envelope.

In the presence of dispersive effects at ion scales, Alfvénic solitons and wave packets can become unstable to parametric modulational instability, leading to steepening and enhancement of  $|B|$  perturbations (Buti et al. 2000). At ion scales, this steepening can produce parallel electric fields capable of efficiently accelerating ions, potentially forming proton beams (Matteini et al. 2010; Gonzales et al. 2021), thereby contributing significantly to ion kinetics in space plasmas. The generation of these structures through parametric decay instability (Derby 1978; Goldstein 1978) aligns with their observed opposite cross-helicity, indicative of sunward propagation, relative to background solar wind Alfvénic fluctuations.

Under quasi-parallel propagation with respect to the magnetic field, Alfvénic solitons are expected to exhibit positive correlations between magnetic field magnitude and density fluctuations for  $\beta < 1$  (Spangler & Sheerin 1982; Buti et al. 2000). However, for sufficiently oblique propagation angles, these structures can maintain anti-correlated  $\delta n$ - $\delta B$  fluctuations, even at  $\beta \sim 1$ , suggesting pressure balance (Baumgärtel et al. 2007). This may explain our events, observed with a significant  $k_{\perp}$  component as discussed in Section 3.3. Under quasi-parallel propagation, quasi-arc polarized solitons degrade rapidly with slight field enhancements, whereas circularly polarized solitons initially exhibit density dips that later positively correlate with the magnetic field (Baumgärtel et al. 2007). This could explain why our observations predominantly capture quasi-perpendicular events, as our event selection criteria, which prioritize significant field enhancements, likely exclude quasi-parallel events from the dataset. Meanwhile, this significant  $k_{\perp}$  component suggests a potential connection to Alfvén vortices (Alexandrova et al. 2006), which are a notable subset of coherent structures in the slow solar wind (Perrone et al. 2016). However, while some similarities exist with the events studied by Perrone et al. (2016); Alexandrova et al. (2013), our analysis does not apply any band-pass filtering to isolate signals from the overall fluctuation spectrum, making it unclear whether they are precisely the same class of structures.

The clustering of these events near the Sun and their distinct properties may be linked to the large-amplitude anti-sunward propagating fluctuations, dominated by switchbacks in the inner heliosphere, as observed by Bale et al. (2019) and Kasper et al. (2019). Parametric decay of these fluctuations (e.g., Matteini et al. 2010; Shi et al. 2017; Bowen



et al. 2018) could generate compressive, sunward-propagating structures, as seen here. The peak occurrence rate near  $\sim 30R_S$ , as suggested by Figure 3 (a), might correspond to the growth and saturation of  $\delta B/B \approx 1$  switchbacks around this distance (Huang et al. 2023). These events may occur more frequently than switchbacks closer to the Sun but become less frequent farther out. However, no definitive conclusions can be drawn, leaving a direct investigation of the correlation between their occurrence rates as future work. The apparent decay of these structures beyond 0.1 AU may result from interactions with background fluctuations. With opposite propagation senses, these structures likely interact with switchbacks, decaying in the process while potentially triggering energy transfer within the switchbacks themselves, thereby contributing to the turbulent cascade. Such events might represent transient mediators of the decay process, contributing to the conversion of switchbacks into a broadband turbulent cascade (Horbury et al. 2023) that ultimately heats and drives the solar wind (Raouafi et al. 2023).

In summary, this study provides clear evidence for the existence of Alfvénic ion-scale solitary structures in the solar wind, observed by Solar Orbiter and Parker Solar Probe. However, ambiguity remains regarding their precise classification and origin, necessitating further theoretical and observational work to explore the relationship between oblique Alfvénic solitons, Alfvén wave packets, and Alfvén vortices at ion scales. Their prevalence at smaller heliocentric distances and their relation with switchbacks deserve further investigation. Most importantly, the apparent sunward propagation of these structures and their abundance in the solar wind suggest potential interactions with the dominant outward-propagating plasma flows, indicating mechanisms for energy transfer or dissipation. This necessitates further work to fully understand their generation mechanisms and their roles in solar wind turbulence.

## 5. ACKNOWLEDGMENTS

Solar Orbiter magnetometer operations are funded by the UK Space Agency (grant ST/X002098/1). Yang and Horbury were supported by STFC grant ST/W001071/1. The RPW instrument has been designed and funded by CNES, CNRS, the Paris Observatory, the Swedish National Space Agency, ESA-PRODEX and all the participating institutes.

## 6. USE OF LIBRARIES AND TOOLS

This study utilized open-source libraries and scientific computing tools, including NumPy (Harris et al. 2020), pandas (Reback et al. 2020), SciPy (Virtanen et al. 2020), Matplotlib (Hunter 2007), SunPy (Community et al. 2020), scikit-learn (Pedregosa et al. 2011), and TensorFlow (Abadi et al. 2016).

## REFERENCES

- Abadi, M., Barham, P., Chen, J., et al. 2016, TensorFlow: A System for Large-Scale Machine Learning. <https://arxiv.org/abs/1605.08695>
- Alexandrova, O., Chen, C. H. K., Sorriso-Valvo, L., Horbury, T. S., & Bale, S. D. 2013, Space Science Reviews, 178, 101, doi: [10.1007/s11214-013-0004-8](https://doi.org/10.1007/s11214-013-0004-8)
- Alexandrova, O., Mangeney, A., Maksimovic, M., et al. 2006, Journal of Geophysical Research: Space Physics, 111, 2006JA011934, doi: [10.1029/2006JA011934](https://doi.org/10.1029/2006JA011934)
- Bale, S. D., Kellogg, P. J., Mozer, F. S., Horbury, T. S., & Reme, H. 2005, Physical Review Letters, 94, 215002, doi: [10.1103/PhysRevLett.94.215002](https://doi.org/10.1103/PhysRevLett.94.215002)
- Bale, S. D., Goetz, K., Harvey, P. R., et al. 2016, Space Science Reviews, 204, 49, doi: [10.1007/s11214-016-0244-5](https://doi.org/10.1007/s11214-016-0244-5)
- Bale, S. D., Badman, S. T., Bonnell, J. W., et al. 2019, Nature, 576, 237, doi: [10.1038/s41586-019-1818-7](https://doi.org/10.1038/s41586-019-1818-7)
- Baumgärtel, K., Sauer, K., Mjølhus, E., & Dubinin, E. 2007, Journal of Geophysical Research: Space Physics, 112, 2007JA012557, doi: [10.1029/2007JA012557](https://doi.org/10.1029/2007JA012557)
- Biskamp, D. 2003, Magnetohydrodynamic turbulence (Cambridge University Press)
- Bowen, T. A., Badman, S., Hellinger, P., & Bale, S. D. 2018, The Astrophysical Journal Letters, 854, L33, doi: [10.3847/2041-8213/aaabbe](https://doi.org/10.3847/2041-8213/aaabbe)
- Breiman, L. 2001, Machine learning, 45, 5
- Bruno, R., & Carbone, V. 2013, Living Reviews in Solar Physics, 10, doi: [10.12942/lrsp-2013-2](https://doi.org/10.12942/lrsp-2013-2)
- Buti, B., Velli, M., Liewer, P. C., Goldstein, B. E., & Hada, T. 2000, Physics of Plasmas, 7, 3998, doi: [10.1063/1.1289890](https://doi.org/10.1063/1.1289890)
- Cattani, C. 2004, Mathematical and Computer Modelling, 39, 255, doi: [10.1016/S0895-7177\(04\)90010-6](https://doi.org/10.1016/S0895-7177(04)90010-6)
- Community, T. S., et al. 2020, The Astrophysical Journal, 890, 68, doi: [10.3847/1538-4357/ab4f7a](https://doi.org/10.3847/1538-4357/ab4f7a)

- Derby, Jr., N. F. 1978, *The Astrophysical Journal*, 224, 1013, doi: [10.1086/156451](https://doi.org/10.1086/156451)
- Frisch, U. 1995, *Turbulence: the legacy of AN Kolmogorov* (Cambridge university press)
- Goldstein, M. L. 1978, *The Astrophysical Journal*, 219, 700, doi: [10.1086/155829](https://doi.org/10.1086/155829)
- Gonzales, C., Klein, K., TenBarge, J., & Howes, G. 2021, *The Astrophysical Journal*, 915, 1
- Greco, A., Matthaeus, W. H., Perri, S., et al. 2018, *Space Science Reviews*, 214, 1, doi: [10.1007/s11214-017-0435-8](https://doi.org/10.1007/s11214-017-0435-8)
- Greco, A., & Perri, S. 2014, *The Astrophysical Journal*, 784, 163, doi: [10.1088/0004-637X/784/2/163](https://doi.org/10.1088/0004-637X/784/2/163)
- Harris, C. R., Millman, K. J., Van Der Walt, S. J., et al. 2020, *Nature*, 585, 357, doi: [10.1038/s41586-020-2649-2](https://doi.org/10.1038/s41586-020-2649-2)
- Horbury, T. S., O'Brien, H., Carrasco Blazquez, I., et al. 2020, *Astronomy & Astrophysics*, 642, A9, doi: [10.1051/0004-6361/201937257](https://doi.org/10.1051/0004-6361/201937257)
- Horbury, T. S., Bale, S. D., McManus, M. D., et al. 2023, *Physics of Plasmas*, 30, doi: [10.1063/5.0123250](https://doi.org/10.1063/5.0123250)
- Huang, Z., Sioulas, N., Shi, C., et al. 2023, *The Astrophysical Journal Letters*, 950, L8, doi: [10.3847/2041-8213/acd7f2](https://doi.org/10.3847/2041-8213/acd7f2)
- Hunter, J. D. 2007, *Computing in Science & Engineering*, 9, 90, doi: [10.1109/MCSE.2007.55](https://doi.org/10.1109/MCSE.2007.55)
- Kasper, J. C., Abiad, R., Austin, G., et al. 2016, *Space Science Reviews*, 204, 131, doi: [10.1007/s11214-015-0206-3](https://doi.org/10.1007/s11214-015-0206-3)
- Kasper, J. C., Bale, S. D., Belcher, J. W., et al. 2019, *Nature*, 576, 228, doi: [10.1038/s41586-019-1813-z](https://doi.org/10.1038/s41586-019-1813-z)
- Khotyaintsev, Yu. V., Graham, D. B., Vaivads, A., et al. 2021, *Astronomy & Astrophysics*, 656, A19, doi: [10.1051/0004-6361/202140936](https://doi.org/10.1051/0004-6361/202140936)
- Kolmogorov, A. N. 1941, *Numbers*. In *Dokl. Akad. Nauk SSSR*, 30, 301
- Leamon, R. J., Matthaeus, W. H., Smith, C. W., & Wong, H. K. 1998, *The Astrophysical Journal*, 507, L181, doi: [10.1086/311698](https://doi.org/10.1086/311698)
- Lion, S., Alexandrova, O., & Zaslavsky, A. 2016, *The Astrophysical Journal*, 824, 47, doi: [10.3847/0004-637X/824/1/47](https://doi.org/10.3847/0004-637X/824/1/47)
- Maksimovic, M., Bale, S. D., Chust, T., et al. 2020, *Astronomy & Astrophysics*, 642, A12, doi: [10.1051/0004-6361/201936214](https://doi.org/10.1051/0004-6361/201936214)
- Matteini, L., Landi, S., Velli, M., & Hellinger, P. 2010, *Journal of Geophysical Research: Space Physics*, 115, 2009JA014987, doi: [10.1029/2009JA014987](https://doi.org/10.1029/2009JA014987)
- Matthaeus, W. H., & Velli, M. 2011, *Space Science Reviews*, 160, 145, doi: [10.1007/s11214-011-9793-9](https://doi.org/10.1007/s11214-011-9793-9)
- Miao, W., Peng, B., Li, Y., & Zhou, L. 2011, *Physics of Plasmas*, 18, 112306
- Mjølhus, E. 1976, *Journal of Plasma Physics*, 16, 321, doi: [10.1017/S0022377800020249](https://doi.org/10.1017/S0022377800020249)
- Osman, K. T., Matthaeus, W. H., Greco, A., & Servidio, S. 2011, *The Astrophysical Journal*, 727, L11, doi: [10.1088/2041-8205/727/1/L11](https://doi.org/10.1088/2041-8205/727/1/L11)
- Osman, K. T., Matthaeus, W. H., Hnat, B., & Chapman, S. C. 2012, *Physical Review Letters*, 108, 261103, doi: [10.1103/PhysRevLett.108.261103](https://doi.org/10.1103/PhysRevLett.108.261103)
- Owen, C., Bruno, R., Livi, S., Louarn, P., et al. 2020, *Astronomy & Astrophysics*, 642, A16, doi: [10.1051/0004-6361/201937259](https://doi.org/10.1051/0004-6361/201937259)
- Pedregosa, F., Varoquaux, G., Gramfort, A., et al. 2011, *Journal of Machine Learning Research*, 12, 2825, doi: [10.5555/1953048.2078195](https://doi.org/10.5555/1953048.2078195)
- Perri, S., Goldstein, M. L., Dorelli, J. C., & Sahraoui, F. 2012, *Physical Review Letters*, 109, 191101, doi: [10.1103/PhysRevLett.109.191101](https://doi.org/10.1103/PhysRevLett.109.191101)
- Perrone, D., Alexandrova, O., Mangeney, A., et al. 2016, *The Astrophysical Journal*, 826, 196, doi: [10.3847/0004-637X/826/2/196](https://doi.org/10.3847/0004-637X/826/2/196)
- Perrone, D., Alexandrova, O., Roberts, O. W., et al. 2017, *The Astrophysical Journal*, 849, 49, doi: [10.3847/1538-4357/aa9022](https://doi.org/10.3847/1538-4357/aa9022)
- Raouafi, N. E., Matteini, L., Squire, J., et al. 2023, *Space Science Reviews*, 219, 8, doi: [10.1007/s11214-023-00952-4](https://doi.org/10.1007/s11214-023-00952-4)
- Reback, J., McKinney, W., et al. 2020, *Zenodo*, doi: [10.5281/zenodo.3509134](https://doi.org/10.5281/zenodo.3509134)
- Rees, A., Balogh, A., & Horbury, T. S. 2006, *Journal of Geophysical Research: Space Physics*, 111, 2005JA011555, doi: [10.1029/2005JA011555](https://doi.org/10.1029/2005JA011555)
- Roberts, O. W., Li, X., & Li, B. 2013, *The Astrophysical Journal*, 769, 58, doi: [10.1088/0004-637X/769/1/58](https://doi.org/10.1088/0004-637X/769/1/58)
- Ryutova, M., & Hagenaar, H. 2007, *Solar Physics*, 246, 281, doi: [10.1007/s11207-007-0399-z](https://doi.org/10.1007/s11207-007-0399-z)
- Shi, M., Li, H., Xiao, C., & Wang, X. 2017, *The Astrophysical Journal*, 842, 63, doi: [10.3847/1538-4357/aa71b6](https://doi.org/10.3847/1538-4357/aa71b6)
- Smith, C. W., Hamilton, K., Vasquez, B. J., & Leamon, R. J. 2006, *The Astrophysical Journal*, 645, L85, doi: [10.1086/506151](https://doi.org/10.1086/506151)
- Sonnerup, B. U. 1998, *Analysis methods for multi-spacecraft data*, 1, 185
- Soucek, J., & Escoubet, C. P. 2008, *Journal of Geophysical Research: Space Physics*, 113
- Spangler, S. R., & Sheerin, J. P. 1982, *Journal of plasma physics*, 27, 193
- Verscharen, D., Klein, K. G., & Maruca, B. A. 2019, *Living Reviews in Solar Physics*, 16, 5, doi: [10.1007/s41116-019-0021-0](https://doi.org/10.1007/s41116-019-0021-0)

Virtanen, P., Gommers, R., Oliphant, T. E., et al. 2020,  
Nature Methods, 17, 261, doi: [10.1038/s41592-019-0686-2](https://doi.org/10.1038/s41592-019-0686-2)

Winterhalter, D., Neugebauer, M., Goldstein, B. E., et al.  
1994, Journal of Geophysical Research: Space Physics,  
99, 23371, doi: [10.1029/94JA01977](https://doi.org/10.1029/94JA01977)

Yao, S., He, J.-S., Tu, C.-Y., Wang, L.-H., & Marsch, E.  
2013, The Astrophysical Journal, 776, 94,  
doi: [10.1088/0004-637X/776/2/94](https://doi.org/10.1088/0004-637X/776/2/94)

Zhang, T. L., Baumjohann, W., Russell, C. T., et al. 2009,  
Journal of Geophysical Research: Space Physics, 114,  
2009JA014103, doi: [10.1029/2009JA014103](https://doi.org/10.1029/2009JA014103)